Reliability with Renewable Energy

STRATEGY ABOUT SYSTEM ADEQUACY AND RESERVE MARGIN WITH INCREASING LEVELS OF VARIABLE GENERATION

Report	WORK PACKAGE 2 – RE predictability and the need for reserves (WASA, CorWind)
Authors	Poul Sørensen, Marisciel Litong-Palima, Mattia Marinelli and Andrea N. Hahmann
Prepared for	Danish-South African Renewable Energy Programme
Date	10 August 2016

Contact Details

Name	Poul Sørensen
Title	Professor
Cell Phone	+45 2136 2766
E-mail	posq@dtu.dk

Technical University of Denmark
Department of Wind Energy
Risø Campus
Frederiksborgvej 399
Building 118
4000 Roskilde
www.dtu.dk

Reviewed by

- Project leader Mikael Togeby, Partner – Ea Energy Analyses, Denmark, mt@eaea.dk
- Project participant Schalk Heunis, EOH Enerweb, Schalk Heunis, schalk.heunis@gmail.com

Glossary of Definitions, Terms and Abbreviations

ACE	Area control error
AGC	Automatic generator control
CorWind	Correlated Wind power time series simulator (DTU Wind Energy software)
D	WT rotor diameter
DoE	Department of Energy, South Africa
Elbas	Nordic intra-day balancing market
IPP	Independent power producer
MTS	Main transformer stations in the ESKOM grid
NOIS	Nordic Operation Information System
PSD	Power spectral density
RE	Renewable energy
WASA	Wind Atlas for South Africa
WP	Work package of the project
WPP	Wind power plant – also known as “wind farm”
WRF	Weather Research and Forecasting
WT	Wind turbine

Contents

Contents

Figures

Tables

1. Introduction

According to the Department of Energy (DoE), South Africa has taken off on a new trajectory of sustainable growth and development, illustrated by the growth of wind and PV generation from 48 GWh/m in January 2014 to 343 GWh/m in December 2014 [1]. For comparison, the electricity consumption was 231 TWh/y in 2014 in South Africa [2].

The above mentioned wind and PV generation in 2014 was obtained with approximately 600 MW wind power and 1000 MW solar PV capacity by the end of 2014. This is the first step towards the implementation of the National Development Plan (NDP) for 7 GW wind and solar to be commissioned by 2020 and a minister target of 13.2 GW by 2025 [1].

The study presented in this report is part of the "Reliability with Renewable Energy" project responding to a call for "Strategies about system adequacy and reserve margin with increasing level of variable generation" launched by South African National Energy Development Institute (SANEDI) in 2015. The aim of the project is to analyse the impact of the variable generation on the operation and planning of the future power system in South Africa. This includes an assessment of the present procedures and methodologies in planning for system reserves and system adequacy in the South African power system.

This report is the main deliverables of Work Package 2 (WP2) studying the variability and predictability of the variable generation and whether those characteristics of variable generation will have an impact on the need for reserves to balance wind power forecast errors in the future South African power system. For this purpose, tools and methods developed and used in cooperation with Danish and European transmission system operators have been applied taking into account the specific South African conditions in the present work.

WP2 should be seen in the project context where WP1 provides a literature review of the system reserves in the South African power system and of international practices and studies [3] and WP3 focus on system adequacy of generation and transmission capacity. In this context, the main objectives of WP2 are to provide time series of the variable renewable generation as input to the adequacy studies in WP3 and to assess the use of the short term or online reserves to balance the RE generation variability.

An important condition for the WP2 work has been to take advantage of the data provided by the Wind Atlas for South Africa (WASA) The WASA project has not only provided information about the spatial distribution of the wind resources in South Africa, but also provided mesoscale time series of wind and solar variability quantifying the temporal variability in addition to the spatial variability. The work in WP2 is based on those WRF simulations.

Section 2 of the report describes the WRF time series used in the present studies. They are based on the original WASA simulations, but minor modifications have been made to include all of South Africa and to include the solar data.

Section 3 describes the estimation of wind power curves based on historical data for wind power generation in existing WPPs. It should be noted that those power curves are providing the relation between WRF wind speeds and WPP power generation, which is different from the conventional wind turbine power curve published by manufacturers because of down scaling, wake effect etc.

Section 4 describes the simulation of wind power time series using DTU Wind Energy's CorWind software. CorWind is simulation wind power time series with a higher temporal resolution than the WRT data, and also provides wind power forecast time series in addition to the real wind power generation time series.

Section 5 describes the simulation of solar time series using DTU CEE's model for PV generation. This is done with the same WRF data as the wind power simulations ensuring the consistent correlation between simulated solar power and wind power.

Section 6 studies the use of the short term or online reserves to balance the variability and forecast errors of wind power generation. In agreement with the project description, solar PV is not included in this study because PV forecast errors are not simulated and because the temporal resolution is higher for the wind simulations (5min) than for the PV simulations (1h).

Finally, Section 7 provides the conclusions of the WP2 studies regarding RE power variability, wind power forecast errors and use of reserves to balance forecast errors.

2. WRF time series

This section describes the WRF time series used in the WP2 studies. They are based on the original WASA simulations, but minor modifications have been made to include all of South Africa and to include the solar data.

The meteorological data was produced using a mesoscale reanalysis method, which is often used for obtaining high-resolution climate or climate change information from relatively coarse-resolution global general circulation models or reanalysis. The mesoscale reanalysis uses a limited-area, high-resolution model driven by boundary conditions from the reanalysis. The strength in using the models to fill the observation gaps is that the fields are dynamically consistent and they are defined on a regular grid. Additionally, the models respond to local forcing that adds information beyond what can be represented by the observations.

The mesoscale reanalysis used to generate the meteorological time series uses the National Center for Atmospheric Research (NCAR) Advanced Research Weather Research and Forecasting (ARW-WRF) model [4]. The version used is v3.5.1 that was released 23 September 2013. The model forecasts use 41 vertical levels from the surface to the top of the model located at 50 HPa; 12 of these levels are placed within 1000 m of the surface. The model setup uses standard physical parameterizations including the Mellor-Yamada (MYJ) PBL scheme [5].

The model was integrated within the domain shown in Figure 1. The outer domain (1) has a horizontal spacing of 30 km x 30 km. The inner domain (2) model grid has a horizontal spacing of 10 km x 10 km, on a lambert projection with center at 29°N, 25°E. The domain has dimensions of 195 × 150 points. The simulation from which the meteorological time series are derived covers 25 years (1990–2014). Individual runs are re-initialized every 11 days. Each run overlaps the previous one by 24 h, to avoid using the time during which the model is spinning up mesoscale processes. A similar method was used and verified in [6], [7], [8]. Initial, boundary, and grids for nudging are supplied by the ERA Interim Reanalysis [9].

Sea surface temperatures (SSTs) that evolve with time, which are derived from satellite and in situ measurements are also used in the simulation. These fields are at a horizontal resolution of 0.25° × 0.25° latitude vs. longitude [10]. They replace the coarse resolution SSTs available from the reanalysis (0.7° × 0.7°) and should adequately represent the horizontal structure and time evolution of the SSTs in this area.

New output fields not available in the standard model were added to the simulation. These include: hourly-averaged wind speed, hourly-averaged kinetic energy flux, and hourly-integrated solar insolation.

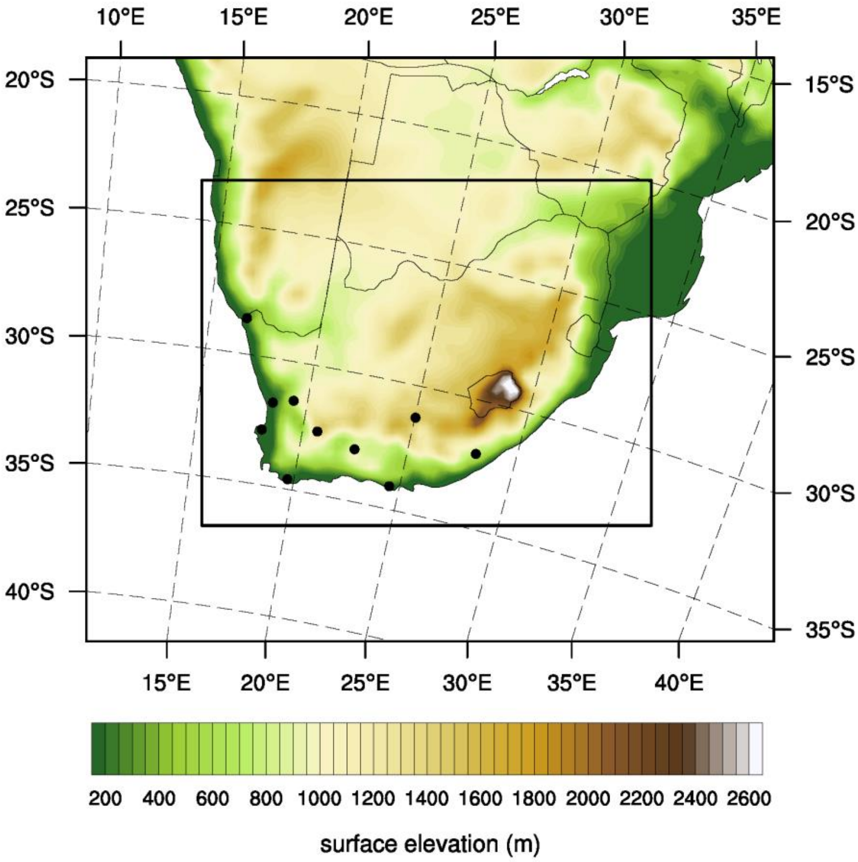

Figure 1: Domain configuration and terrain elevation used in the simulations. The circles show the location of the WASA measurement masts.

3. Wind power curves

3.1 Historical wind power generation data

For the purpose of estimating wind power curves, WPP generation time series were extracted from the ESKOM database with 30 minutes resolution. One year (from 26 August 2014 to 25 August 2015) of simultaneous generation data was available from each of the eight WPPs with the locations shown on the map Figure 2. Therefore, those WPPs have been used for the estimation of power curves.

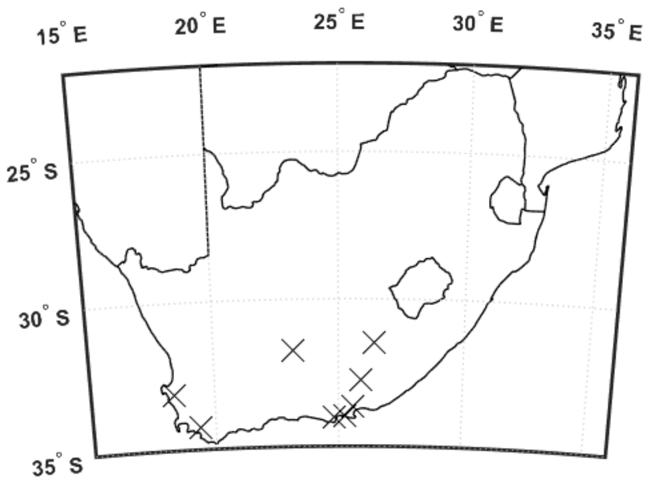

Figure 2: Location of WPPs with historical generation data.

3.2 Methodologies for power curve estimation

The purpose of estimating power curves from historical WPP data is to be able to use the power curves for to simulate WPP generation time series using WRF time series as input. Therefore, the estimated WPP power curves should provide the relation between the wind speeds from the WRF model time series and the WPP power generation. This is noteworthy different from conventional WT power curves, which provide the relation between the wind speed in hub height close to the WT and the WT power.

Figure 3 shows the scatter of simultaneous one hour averages of WRF wind speed and measured power for one of the eight WPPs. This scatter is very high compared to scatter of 10 minute averages used in WT power curves. The main reason for this difference is that the WRF wind speed time series are modelled whereas the measured WT wind speeds are measured closely to the WT.

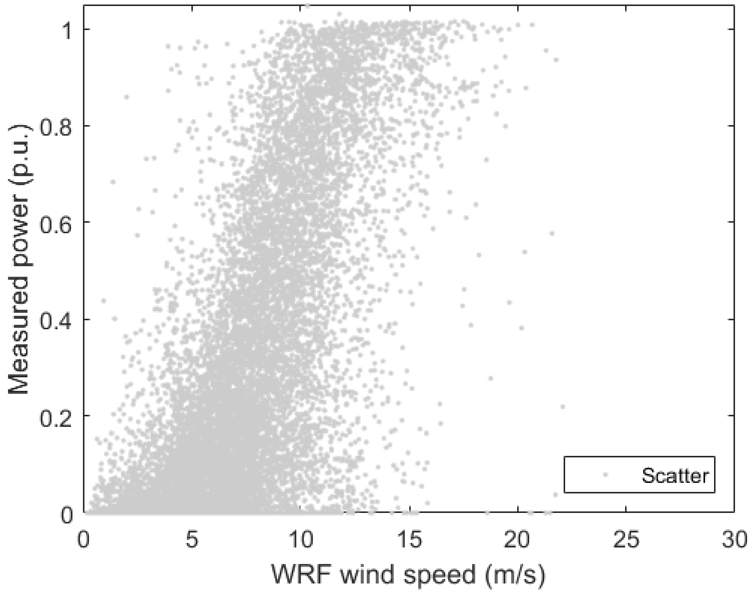

Figure 3: Example of power curve 1h scatter data.

Figure 4 shows the estimated power curve using the standard method of bin which is e.g. specified in the WT power curve standard IEC 61400-12-1 [11]. In short, this method first divides the wind speed axis into intervals or bins, then each pair of wind speed / power data is sorted into those bins, and finally the average wind speed and average power is calculated in each bin. The result shows that with the present very high scatter, it is questionable to use this power curve. For instance, the maximum power is less than 0.9 p.u. for the binned power curve although the maximum measured power is 1.0 p.u. Using this power curve to simulate WPP power time series would result in an unrealistic probability distribution of the simulated power with maximum power values which are much smaller than the maximum values of the measured power.

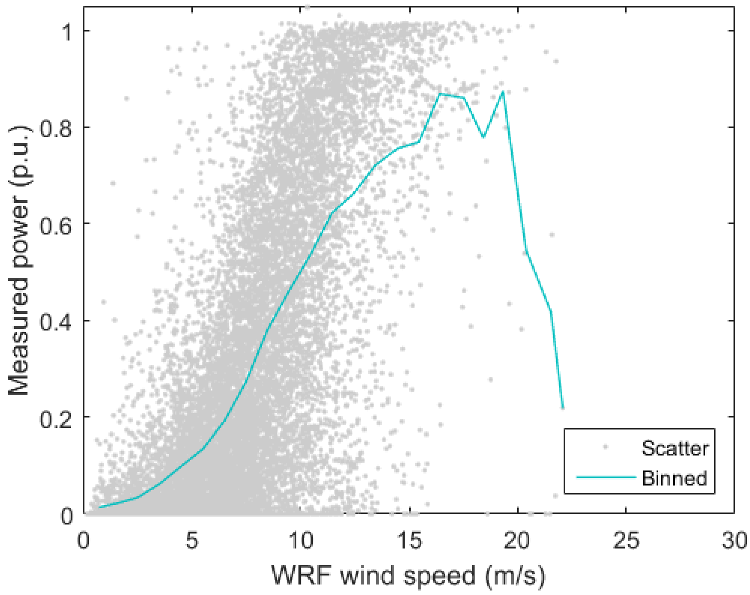

Figure 4: Power curve estimation using method of binning.

Alternatively, the power curve can be derived from the duration curves of WRF wind speeds and measured power respectively as illustrated in Figure 5. The idea is to pair the wind speeds and powers with the same percentile.

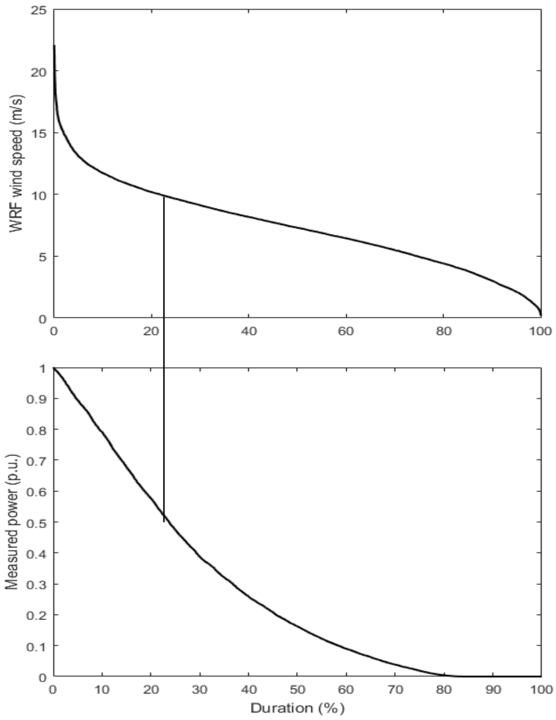

Figure 5: Pairing wind speed and power curves from duration curves.

The power curve estimate using the duration curve method is shown in Figure 6. The advantage of the duration curve method is that the simulated wind power time series will have the same probability distribution as the original measurements. The main disadvantage is that this method assumes that the power curve is monotonic, which means that it neglects the decrease in power at high wind speeds caused by shut downs of wind turbines.

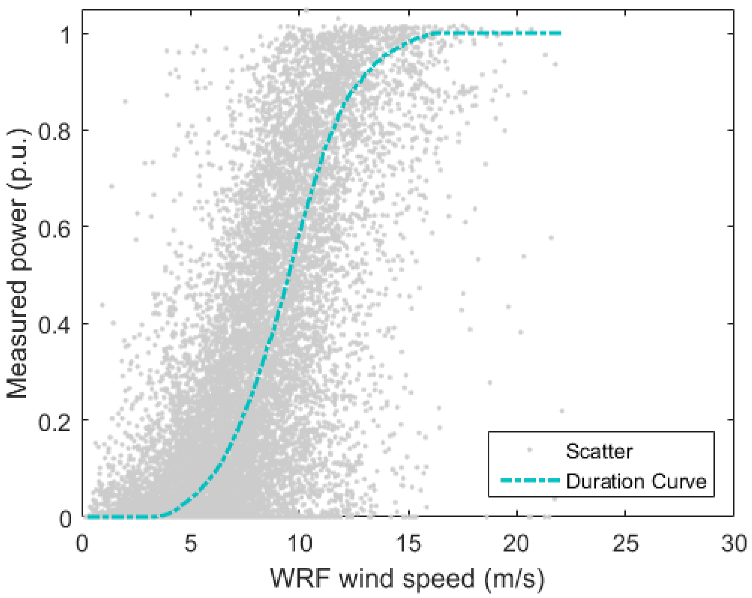

Figure 6: Power curve estimation using the duration curve method.

Finally, it is in principle possible to use numerical wind atlas to downscale the WRF wind speeds to wind speeds at coordinates for individual WTs as illustrated in Figure 7. A fundamental problem with this approach is that that it would require a detailed plan for the positions, not only of future WPPs but of the individual WTs in the WPP. Another issue is that the accuracy of this approach has not yet proven to be higher than the estimation based on measured power from existing WPPs as described above [12].

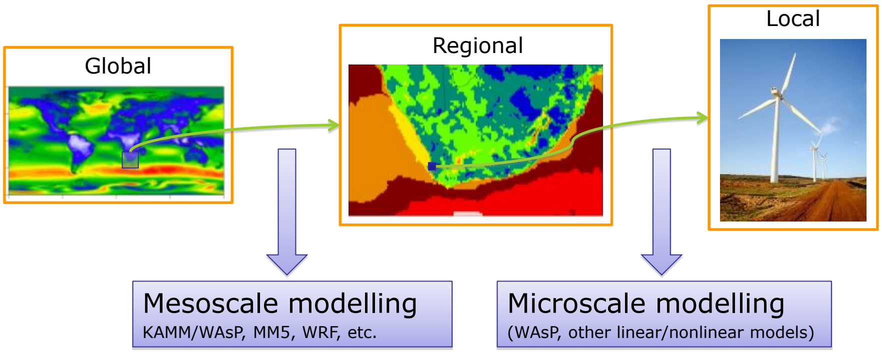

Figure 7: Possible microscale downscaling if location details are known.

3.3 Specific and general power curves

The purpose of this clause is to derive the specific power curves for each of the eight WPPs in Figure 2 and to use the specific power curves to derive a general power curve to be used for other WPPs.

Figure 8 shows the specific power curves for each of the eight WPPs estimated with duration curve methodology. Generally, there are significant differences between the power curves, which illustrates the uncertainties associated with using a general power curve. For the purpose of studying the use of fast reserves to deal with wind power variability, the main objective is to get good accuracy in the sum of wind power from all WPPs in the system. However, in the system adequacy studies the differences between power curves of WPPs connected to different MTS's is expected to have some influence on congestions. However, improvement of the accuracy using microscale downscaling as illustrated in Figure 7 would require detailed plans for WPP and WT siting, and for some sites wind speed measurements would also be necessary as a supplement to the downscaling. On this background, the specification of a general power curve based on estimated individual WPP power curves is considered most the most feasible solution, which was also planned in the proposal stage of the project.

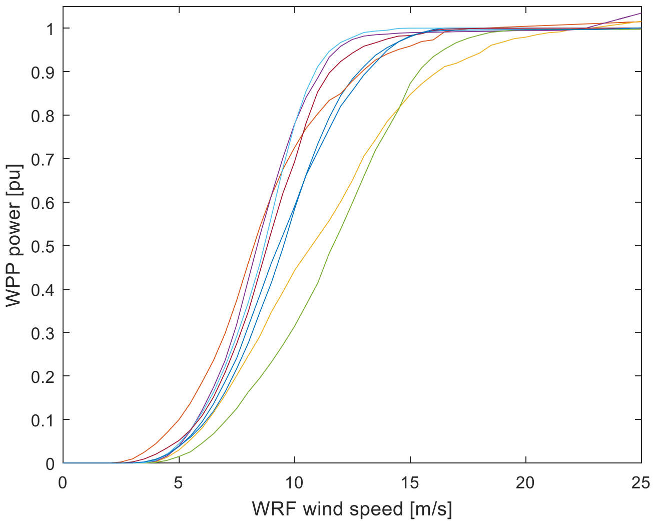

Figure 8: Power curves for each of the WPP estimated with duration curve methodology.

Two of the eight power curves are significantly lower than the remaining six. Since local conditions may explain this difference, it was decided to determine the general power curve as the average of the remaining six power curves. The resulting general power curve is shown in Figure 9 together with the specific WPP power curves.

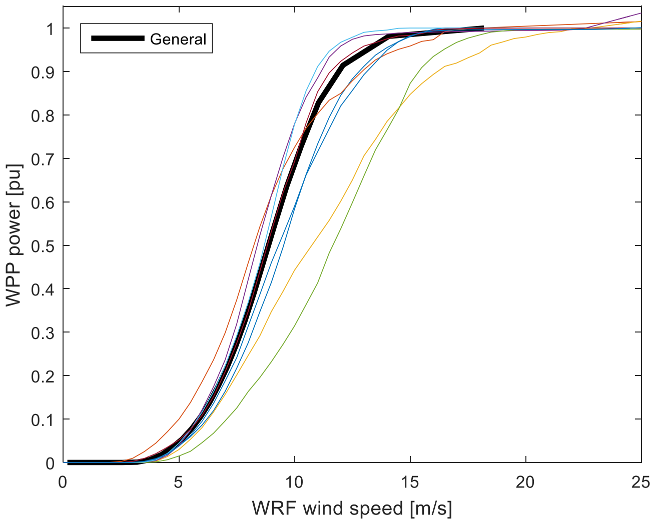

Figure 9: General power curve compared to power curves for WPPs with historical data.

3.4 Specific power normalization of power curves

This section describes a way to normalize power curves depending on the specific power. The work was not foreseen in the SANEDI contract, but it was done as part of an internally funded CorWind development project in DTU [13].

The specific power of a WT is defined as the ratio between the rated power and the rotor area of the WT. The specific power has a significant influence on WT power curves, which is affecting the WPP power curves in a similar way.

The basic assumption of the normalization is that the possible aerodynamic power is proportional to the rotor area, which is evident from (1).

$$P_{\mathrm{aero}} = \frac{1}{2}\rho A V^3 C_p \tag{1}$$

Since the WT controller is able to track the maximum C_p value in the so-called region 2 [14], the WT power curve is approximately cubic until the power is limited. In this region, the electrical power output of the WT can be approximated to

$$P_{\mathrm{el}} = kAV^3 - P_0 \tag{2}$$

where P_0 is the no-load losses.

Figure 10 verifies that (2) also is a very good approximation for the WPP power curve in region 2. The differences outside region 2 occur because the optimal rotational speed is outside the WT speed range, and because Figure 10 is a WPP power curve which is smoother than the originating WT power curve [15].

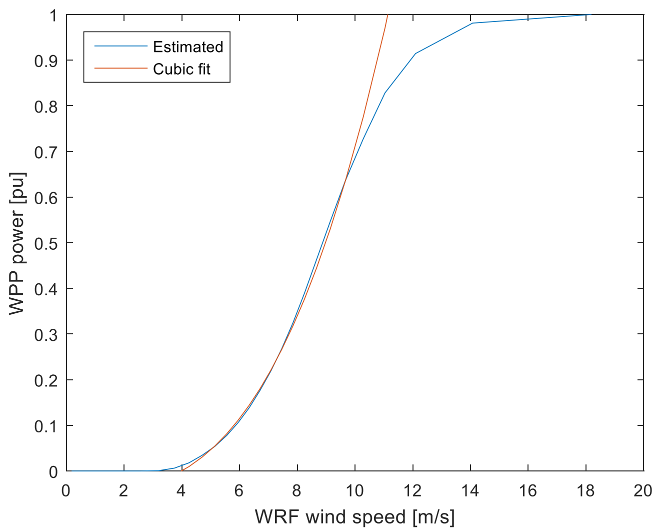

Figure 10: Cubic fit of optimal power region of estimated power curve [13].

The no-load losses can be assumed to be the same for two WTs with the same rated power although the rotor area is different. Now the power of two wind turbines with different areas A_1 and A_2 is the same if

$$A_1{V_1}^3 = A_2{V_2}^3 \qquad (3)$$

Therefore, the power curve of the second WT can be derived from the power curve of the first WT by substitution of the wind speeds

$$V_2 = \sqrt[3]{\frac{A_1}{A_2}}\, V_1 = \sqrt[3]{\frac{\mu_2}{\mu_1}}\, V_1 \qquad (4)$$

where μ denotes the specific power.

This wind speed substitution in (4) is applied to the power curves in Figure 8 normalizing to the common specific power $\mu_1 = 259\ \mathrm{W/m\^2}$. The result is shown in Figure 11. Comparing the figures, it is seen that the power curves are generally a little closer after the normalization, but there is still a significant difference between them.

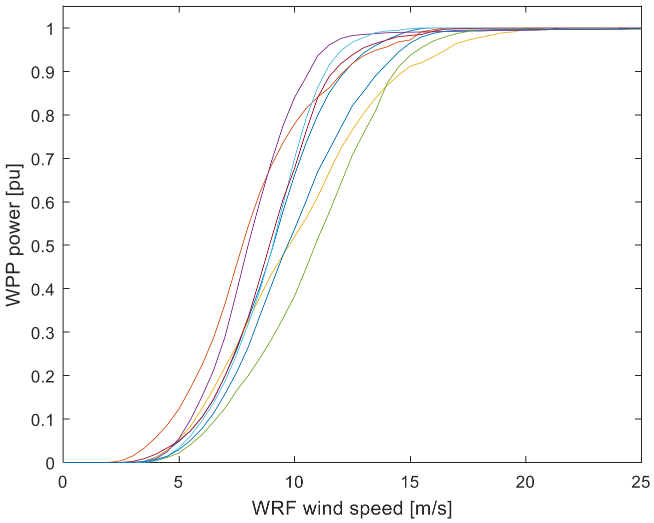

Figure 11: Power curves for each of the WPP normalized to 259 m/W2 [13].

3.5 General power curve for possible future values of specific power.

This wind speed substitution in (4) is now applied to derive general power curves for different values of the specific power. The idea is to specify power curves for additional simulation cases to study the impact of the choice of WTs specific power.

Figure 12 shows the specific power vs. rated power for the South African WPPs in Figure 2 compared to statistical data from IEA Wind Task 26 [16] for WTs installed in European Union 2007 – 2012 and data from DTU Energy Report 2015 for the 10 largest offshore WTs ultimo 2014 [17]. It is noticed that the WTs in South Africa already have quite low specific power values compared to the averages for European Union and for the largest offshore wind turbines.

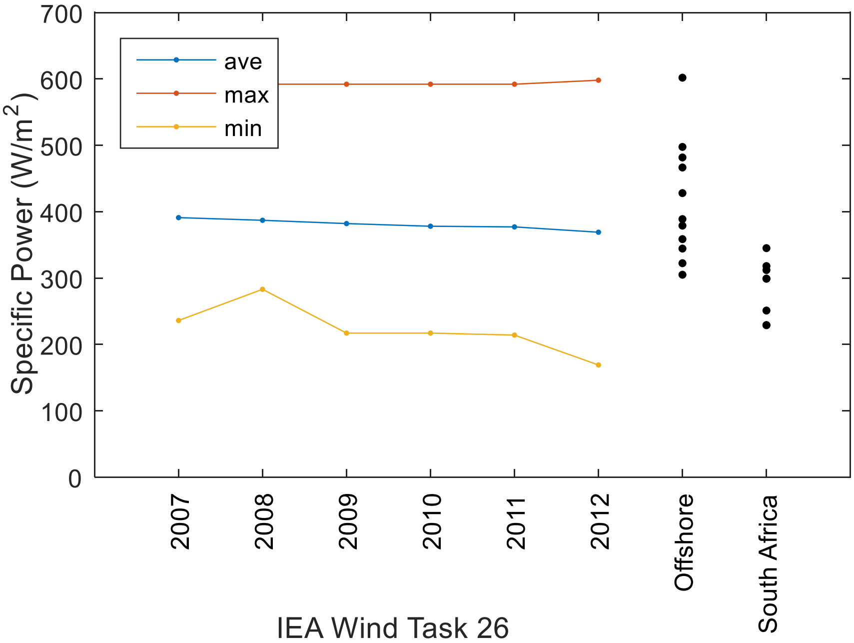

Figure 12: Specific power of WTs in South Africa compared to other sources.

Figure 13 shows the WPP power curves for the following values of specific power:

- 259 W/m2 which is the average for the general power curve in Figure 9.
- 229 W/m2 being the present minimum specific power for WTs in South Africa
- 196 W/m2 being a very low but existing WT specific power, corresponding to 2.0 MW rated power with 114m diameter rotor.

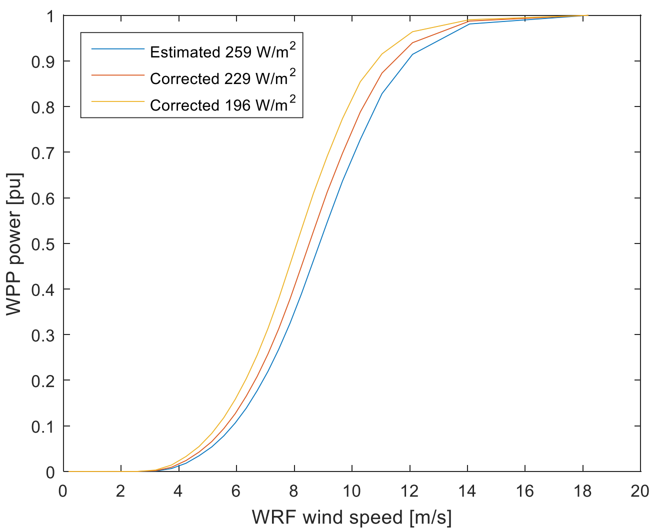

Figure 13: Corrected power curves for different values of specific power (W/m^2) [13].

4. Wind power time series simulations

This section describes the simulation of wind power time series using DTU Wind Energy's CorWind software. CorWind is simulation wind power time series with a higher temporal resolution than the WRT data, and also provides wind power forecast time series in addition to the real wind power generation time series. The time series generation described in this section are used for the assessment of the use of reserves in section 6, and in the assessment of the system adequacy in WP3.

4.1 CorWind methodology

4.1.1 General description

CorWind is an advanced tool developed at DTU Wind Energy for simulation of wind power time series used in power system planning studies. The methods implemented in CorWind take into account the spatial and temporal correlations ensuring a realistic representation of the smoothing effects caused by the spatial distribution. This is validated using real data from areas in the Danish power system [18].

CorWind has been used in a number of studies, including the following main references:

- Assessment of the market and system impact of large scale offshore wind power in the future (2020 and 2030) North European power system as part of the EU TWENTIES project, with special focus on wind power storm control and balancing with Nordic hydro power [19].
- Simulation of balancing (Simba) in the Danish power system, led by the Danish TSO Energinet.dk in cooperation with DTU [20].
- ENTSO-E's ongoing work on a new Ten Years Network Development Plan (TYNDP) [21].
- Assessment of the need for automatic reserves in European synchronous areas to balance future (2020 and 2030) wind power [22].

CorWind is capable of simulating consistent time series of wind power production and prognosis as illustrated for a Danish offshore 2020 case in Figure 14, where a set of simulated real time wind power production P_W_RT, day-ahead prognoses P_W_DA and hour-ahead prognoses P_W_HA are shown.

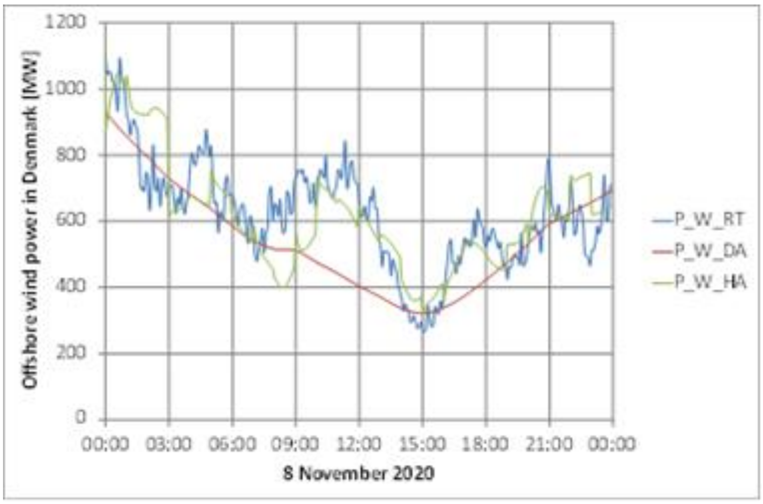

Figure 14: Example of CorWind simulation of real time wind power production P_W_RT, day-ahead prognoses P_W_DA and hour-ahead prognoses P_W_HA.

CorWind is considered the best solution for the purpose of assessing the needs for reserves due to wind power variability and uncertainty, because CorWind is developed to simulate realistic wind power ramp rates and wind power forecast errors. Data from Danish offshore WPPs has been used to validate that the simulated fluctuations have ramp rate statistics which are similar to measured ramp rate statistics [23].

Mesoscale weather models like the WRF model used to generate the WASA data generally underestimate the variability in the wind speeds, which has been documented comparing the power spectral densities of measured and mesoscale simulated wind speeds [24]. This missing variability is not only important for extreme wind speeds as pointed out in [24], but also has a significant influence on the ramp rates and forecast errors of wind speeds.

CorWind compensates for the missing variability by adding wind speed fluctuations corresponding to the difference between the fluctuations in the measured wind speeds and the fluctuations in the WRF simulated wind speeds.

Figure 15 shows the power spectral densities (PSDs) of measured wind speeds and WRF simulated wind speeds for a Danish offshore site. The difference between the measured PSD and the WRF PSD is used in CorWind to add the missing variability as random fluctuations.

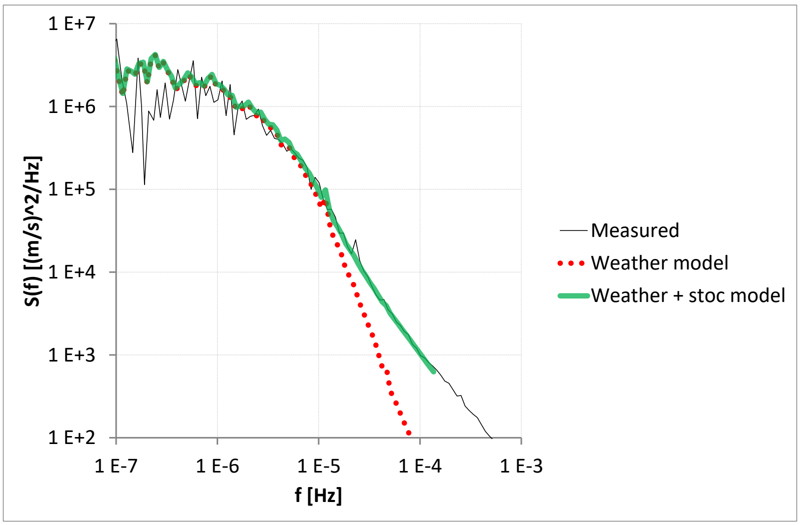

Figure 15: Power spectral densities of 'measured' wind speeds and WRF 30km x 30km resolution 'weather model' simulation for Danish offshore site. CorWind 'Fluctuation model' power spectral density used by CorWind for Denmark is added to the 'weather model'.

The effect of adding the missing variability is illustrated by the time series in Figure 16. The red curve is WRF wind speeds while the blue and green curves are WRF wind speed plus added wind speed fluctuations. From this illustration it is obvious that the added fluctuations are essential to include for quantification of the ramp rates of wind power.

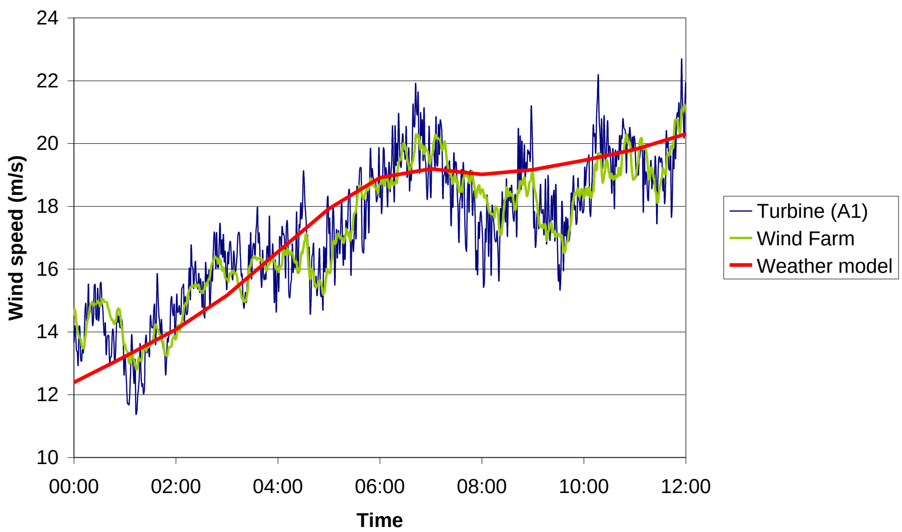

Figure 16: Time series simulated with CorWind. The red curve is WRF wind speeds, the blue curve includes added fluctuations for a wind turbine, and the green curve shows wind speeds averaged over a WPP.

The main structure of CorWind is shown in Figure 17. It is based on a database of meteorological data, which is usually 1 hour resolution data generated with WRF. For South Africa, the updated data from the WASA project will be used.

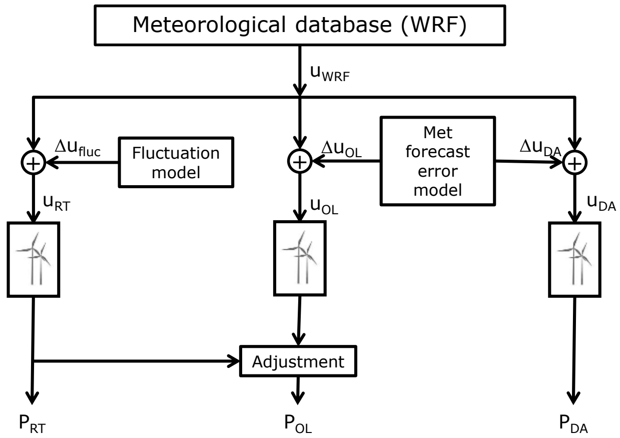

Figure 17: CorWind main structure.

The left branch in Figure 17 provides the real time wind power time series PRT. In order to include wind speed fluctuations which are not captured by the WRF model with the given resolution, CorWind adds randomly generated fluctuations Δu_{RT} to the WRF wind speeds u_{WRF} as illustrated in Figure 16. The applied method is based on a frequency domain approach applying power spectral densities to describe wind speed fluctuations and coherence functions to describe correlations [25]. This frequency domain approach ensures a realistic smoothening when the output power from many wind turbines or WPPs are added.

CorWind uses power curves to convert wind speeds to power, and in the EU TWENTIES project, the simple power curve approach has been extended with a method to include the shut-downs and start-ups due to extreme weather conditions [19].

The right branch in Figure 17 provides the day-ahead wind power time series P_{DA}. It adds a forecast error Δu_{DA} to u_{WRF} to provide the day-ahead wind speed forecast u_{DA}. Δu_{DA} is generated using a multivariate ARMA process [26].

The middle branch in Figure 17 provides the online wind power forecast P_{OL}. This is also simulated using a multivariate ARMA, but with shorter horizon than the day-ahead ARMA. The online forecast also includes an additional adjustment procedure, which ensures that the online forecast is improved based on the knowledge about the actually produced power, which is typically available to the TSO from the SCADA of the energy management system.

The hour-ahead wind power time series P_{HA} shown in Figure 14 is a special case of the online wind power forecast P_{OL}. In this case of hour-ahead forecasts, the online prognosis is called half an hour before the hour of operation, which corresponds to the forecast used by the Danish TSO Energinet.dk to make a plan for balancing the power system using regulating power.

4.1.2 South Africa calibration

This section describes the calibration of the fluctuation model in CorWind. The work is outside the SANEDI contract, but it was done as part of an internally funded CorWind development project in DTU [13].

As mentioned in the general description, the match between the simulated and measured PSDs in Figure 15 were based on wind speed measurements on a Danish offshore site.

Thus, the CorWind fluctuation model (Figure 17) was calibrated to match those measurements.

This calibration has a significant influence on the variability of the simulated wind power time series. Therefore, a similar calibration is performed based on wind speed measurements in South Africa. For this purpose, WASA mast data [27] was used.

Figure 18 shows the PSDs of measured, WRF and CorWind wind speeds for 10 masts in South Africa [13]. The match between measured and CorWind PSDs is obtained by estimating the parameter $a_1 = 5 \cdot 10^{-4}$ for the South Africa data which for comparison was $a_1 = 3 \cdot 10^{-4}$ in the Danish offshore case [24]. This difference can be translated to $\sqrt{5/3} = 1.3$ times larger amplitudes of the fast wind speed fluctuation components which have period times less than $1/(4 \cdot 10^{-4}\text{Hz}) \approx 6 \text{ hours}$.

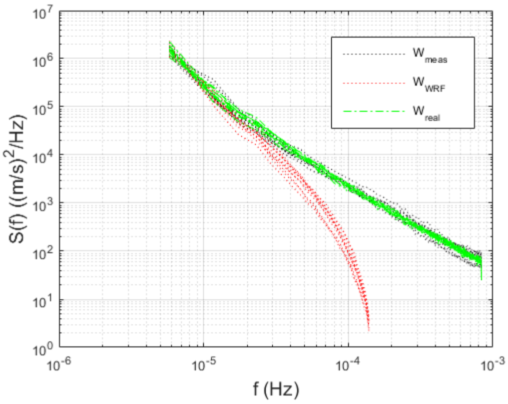

Figure 18: PSDs of measured, WRF and CorWind wind speeds for 10 masts in South Africa [13].

4.1.3 CorWind validation against measured wind power time series in South Africa

The one year wind power data which was used to estimate the power curves in section 3 is now used to validate the ability of CorWind to simulate wind power time series with ramp rates that have probabilistic distributions close to the ramp rates of measured wind power time series.

Figure 19 shows the duration curves of measured and simulated 30 min ramp rates for the sum of wind power from 8 WPPs in Table 1. The 30 min ramp rates are chosen for the comparison because the temporal resolution of the measured wind power time series is 30 min.

Figure 19 shows and excellent agreement between the measured and simulated ramp rate duration curves in the interval from 1% to 99%. In the low probability cases below 1%, there are some deviations. It should be noticed that this very good result is obtained with the specific power curves for the individual 8 WPPs estimated in section 3.3 and the calibration of the fluctuation model in section 4.1.2.

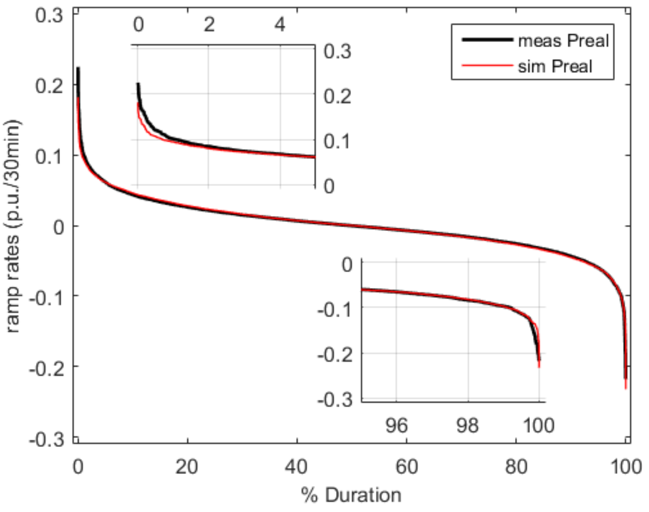

Figure 19: Duration curves of measured and simulated 30 min ramp rates for the sum of wind power from 8 WPPs in Figure 2.

4.2 Simulation cases

Three simulation cases have been defined in agreement with ESKOM and DOE. Those cases are:

- 2014 being the reference (Past) case including the WPPs installed in the beginning of the year.
- 2020 being the (Planned) development case.
- 2025 being a not too far future case to be considered in the grid development plans.

The total installed capacity for the 3 cases are shown in Table 1.

Table 1: Installed capacities for the three simulation years

Case year	2014	2020	2025
Installed capacity [MW]	460	3800	7400

The location of the WPPs in each scenario is shown in Figure 20 based on data from ESKOM. The locations are affecting the correlations and thereby the spatial smoothening of the wind power fluctuations, and therefore used as input to the CorWind simulations. For the 2014 and the 2020 scenarios, the exact positions of the WPPs are known. For the additional WPPs in the 2025 scenario, the exact locations have not been identified at this stage, but the locations of the MTSs are provided.

Based on this data, the WPPs locations are specified as follows: For the WPPs where the locations are known, those are used. For the WPPs where only the MTS location is known, the WRF points with 10 km x 10 km separation are used. For this purpose, the capacities of the planned WPPs are divided into 100 MW units, and each unit is then placed in its own WRF point. The WRF points are selected as the nearest points to the MTS location.

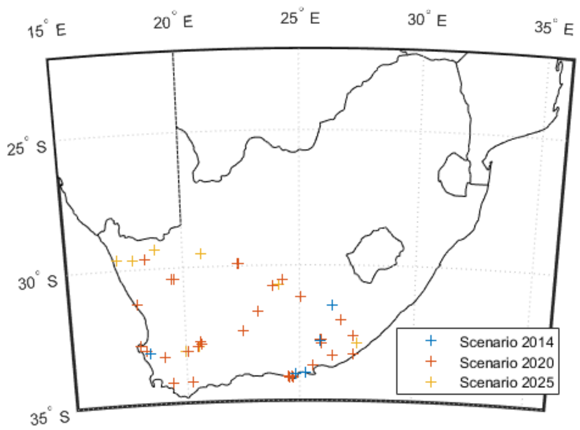

Figure 20: Location of WPPs

4.3 Results using all 25 years of WRF data

The results in this section are based on CorWind simulations of real wind power and wind power forecasts. The simulations of real wind power and of hour-ahead and online prognoses are done with 5min temporal resolution, whereas the smooth day-ahead forecasts are simulated with 1 hour resolution corresponding to the typical resolution of forecast systems.

For the eight WPPs with historical data, the specific power curve for each WPP is used. For the remaining WPPs, the general estimated power curve is used, corresponding to 259 W/m^2 specific powers.

The simulations are done using all 25 years of WRF reanalysis time series. For each year, different random seeds are used to make the stochastic simulations in CorWind. This approach ensures a good coverage of annual as well as seasonal and diurnal variations.

Figure 21 shows the duration curves for each of the scenarios. It is noticed that the generated power in p.u. was significantly lower in 2014 than expected in 2020 and 2025. This is mainly a result of simulating 2014 using all the eight specific power curves in Figure 6 while 2020 and 2025 is simulated using the general power curve in Figure 9 for the remaining majority of WPPs where the power curve is not estimated.

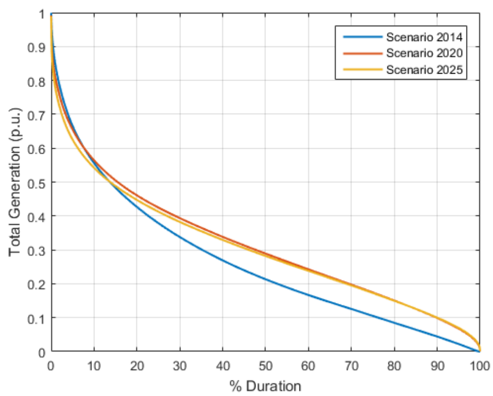

Figure 21: Duration curves of wind power generation.

Another observation in Figure 21 is that the generation in the 2025 scenario is a little less than the other scenarios for the low (0-10%) percentiles. This can be explained by the wind speed distributions which are slightly lower in the 2025 development areas than in the 2020 development areas.

The capacity factors of each scenario are shown in Table 2. The table also shows the corresponding wind power penetration levels assuming the “SO moderate” 2020 and 2025 forecasts of electricity consumption according to the Integrated Resource Plan 2010-2030 [28] which was also used in WP3.

Table 2: Capacity factors and corresponding wind power penetration

Case year	2014	2020	2025
Capacity factor [%]	26.2	31.4	30.5
Consumption [TWh/y]	231	356	404
Penetration [%]	0.5	2.9	4.9

Figure 22 shows the distribution of those capacity factors for the different WRF years. The variations from one WRF year to another simply reflects that some years have higher average wind speeds than other years. For instance, it is seen that the wind speeds in 2014 were higher than average.

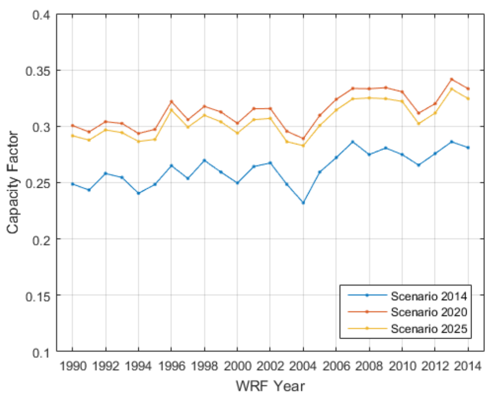

Figure 22: Annual capacity factors for each of the scenarios.

Whereas the results above regarding generation duration curves and capacity factors are mainly affecting the results in WP3 regarding stochastic system adequacy analyses, the main focus in WP2 is on the forecast errors and ramp rates and how those variables affect the use of reserves.

Figure 23 shows the duration curve of the 10 minute ramp rates for each of the scenarios and the corresponding mean absolute values are shown in Table 3. This clearly illustrates that the p.u. (i.e. relative) ramp rates is reduced significantly from the 2014 to the 2020 scenario and further slightly reduced for the 2025 scenario. This is due to the smoothening effect with the WPP locations in Figure 20.

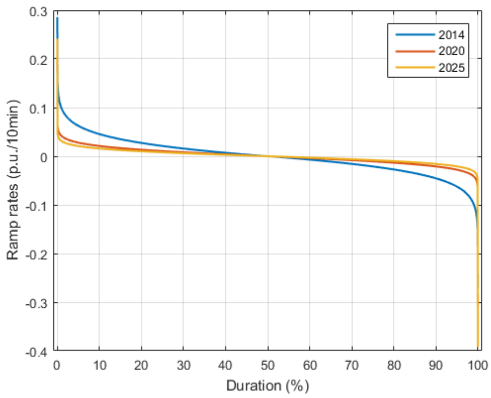

Figure 23: Duration curves of ramp rates.

Table 3: Mean values of absolute ramp rates

Case year	2014	2020	2025
Mean absolute ramp rate [p.u./10 min]	0.028	0.013	0.010

The smoothening effect is also distinct for the duration curves of forecast errors in Figure 24 (day-ahead), Figure 25 (hour-ahead) and Figure 26 (10 minute online forecasts).

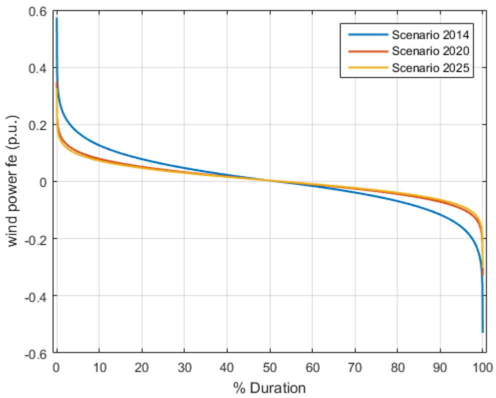

Figure 24: Duration curves of day-ahead forecast errors.

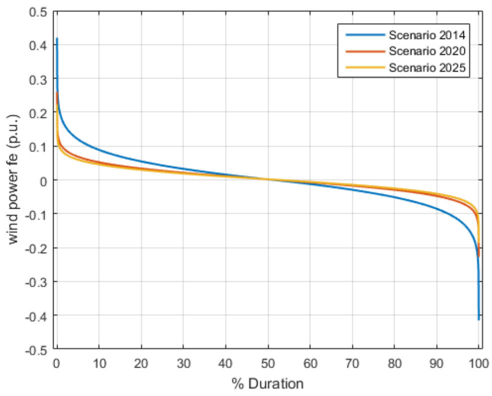

Figure 25: Duration curves of hour-ahead forecast errors.

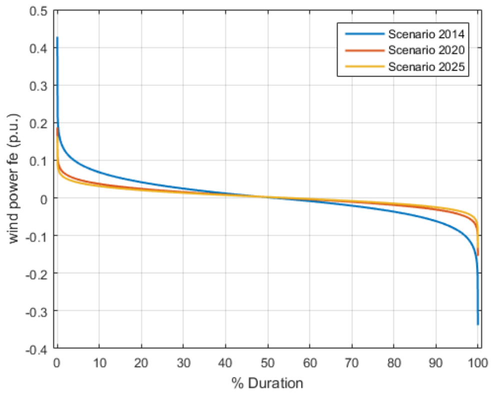

Figure 26: Duration curves of 10-minute online forecast errors.

Table 4 summarizes the mean absolute error the forecast errors for different horizons and different scenario years. Apart from confirming the smoothening effect by comparing the scenario years, the results also show how the forecasts are improved reducing the horizon from day-ahead to hour-ahead and 10-minute online.

Table 4: Mean absolute wind power forecast errors (MAE) in p.u. of installed wind power capacity

Case year	2014	2020	2025
Day-ahead error [p.u.]	0.075	0.047	0.043
Hour-ahead error [p.u.]	0.054	0.031	0.027
Online (10 min) error [p.u.]	0.040	0.021	0.017

Comparing the MAEs of the online 10 min forecast errors in Table 4 to the mean absolute value of the 10 min ramp rates in Table 3, it is observed that the online forecast errors are greater than the ramp rates. This was not expected for the following reason:

The simple so-called persistence forecast predicts the future wind power forecasts to stay equal to the initial value. Therefore, the error of a persistence forecast with a 10 min horizon is equal to minus the 10 min ramp rate. Thus, the error of the persistence forecast is less than the CorWind online forecast simulation.

The performance of the CorWind 10 min online forecast depends on the adjustment procedure, see Figure 17. This is a rather complex procedure depending on parameter choices which were only calibrated for hour-ahead forecasts.

In general, the forecast error should be less than the simple persistence model error. Therefore, the simulated real power is used to quantify the 10 min forecast errors in the following in the following analyses.

4.4 Results for different specific power values

The results in this section are based on CorWind simulations of real wind power done with 5min temporal resolution using WRF reanalysis data from 2014.

Figure 27 shows the duration curves for the 2025 scenario using the power curves for different specific power of new WPPs.

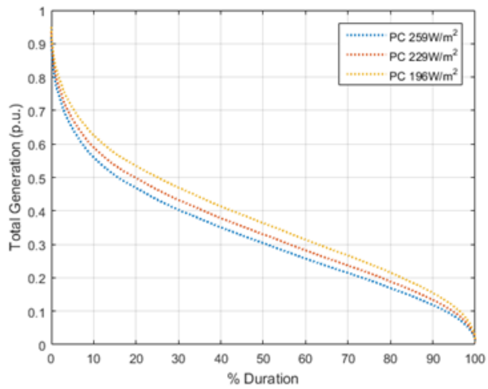

Figure 27: Duration curves for 2025 scenario using different specific power of new WPPs.

Table 5 shows the calculated capacity factors for 2025 corresponding to the duration curves in Figure 27. It is seen that the capacitor factors increase significantly with lower specific power. It is also noted that the capacity factor 0.32 for 259 is a bit higher than the capacity factor for 2025 in Table 2, which is because 25 years of wind speeds were used in Table 2 results while only 2014 wind speeds were used in Table 5 results, and 2014 wind speeds were higher than average.

Table 5: Capacity factors 2025 for different specific power of new wind turbines

Specific power [W/m^2]	**259**	**229**	**196**
Capacity factor	0.32	0.35	0.38

Finally, Figure 28 shows the duration curves for the 10 min ramp rates for different specific powers. It is expected that the ramp rates will increase with lower specific power because the power curves are a little steeper in lower wind speed ranges and because the WTs operate more frequently in this range. On the other hand, the maximum power where the slope is zero is reached earlier when the specific power is low. Figure 28 shows that the changes in ramp rate duration curves are very small.

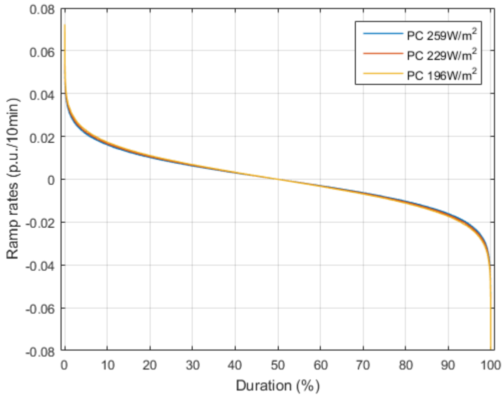

Figure 28: Duration curves for 2025 10 min ramp rates using different specific power of new WPPs.

5. Solar PV simulations

5.1 Methodology

The PV power estimations are based on the WRF time series on hourly basis of selected meteorological parameters for the selected historical period for each 10x10 km^2 areas (MetCells or Tile) of the entire South Africa area described in chapter 2, i.e. with the same WRF runs which are used to generate the wind power time series in chapter 4. Out of the 195 x 150 = 29250 met cells in the inner WRF domain (see Figure 1), normalised PV generation time series are simulated for each of the 11,883 MetCells covering the South Africa area. Subsequently, those time series are aggregated into 176 nodes corresponding to each of the MTS's in South Africa.

Table 6 shows a list of the WRF data used in the PV modelling. The data are averaged values over time (except for the irradiance that is cumulated) and space – over the hour and over the MetCell area.

Table 6: Historical meteorological data

Symbol	Unit	Data
t		Timestamp (date and time)
(x;y)		Longitude and latitude (centre of the MetCell)
N		Transmission node ID (MTS)
U_{10m}	(m/s)	Average wind speed at 10 m height level
T_{air}	(°C)	Average air temperature at 2m above surface level
I	(W/m^2)	Cumulated solar irradiation at surface level and horizontal surface

The estimated AC Normalized solar power output is given as normalised values (in pu). The actual estimated power generations can be found by multiplying the normalised power generation, with the actual installed power capacity for each Transmission Node.

The power generation from a PV panel is a complex function of many parameters. The power generation from a PV panel, P^{PV}_n, depends on the PV technology, and is generally function of the direct solar irradiation, the indirect solar irradiation, and the temperature of the PV panel. The relations are different for the different PV technologies. The temperature of the PV panel is obtained at the balance between heating and cooling of the panel. The panel is heated by the solar irradiation and the internal power losses, and cooled by the heat flux to the ambient. The heat flux to the ambient depends on the air temperature and the air flow, and the air flow depends on the general wind speed and the mounting of the panel. In the present PV model, the estimated wind speed at 10 m height level above the ground has been used as the general wind speed, and the mounting of the PV panels is assumed to be on building rooftops.

The normalised PV power, $P^{PV}_{N,n}$, are estimated for each Transmission Node, N, and for each hour for the time span analysed (1990-2014), based on the meteorological data, the distribution of the installed capacity between the MetCells, the mix of PV technologies and the distribution of the installed PV power between ground based PV and building integrated PV, and different orientations and tilt angles. The distributions of the PV capacities between the MetCells within each Transmission Node are given by capacity factors, $k^{PV}_{N;M}$, for each Transmission Node, N, and each MetCell, M. Default value: 1.

The aggregated, normalised PV power generation for each Node (MTS) is finally calculates as the weighted average power generation of all MetCells within the Node:

$$P_{N;n}^{PV} = \frac{\sum \left(k_{N;M}^{PV} \times P_{N;M;n}^{PV} \right)}{\sum M^{N}} \qquad (5)$$

5.2 PV Model

The model, realized in Simulink (Matlab simulation environment), is formed by several blocks where the equation for the description on the movement of the Sun and the evaluation of the efficiency chain in the energy conversion process of the PV module, starting from the Sunlight getting to the AC normalized output, are implemented.

A conceptual layout of the model is presented in Figure 29.

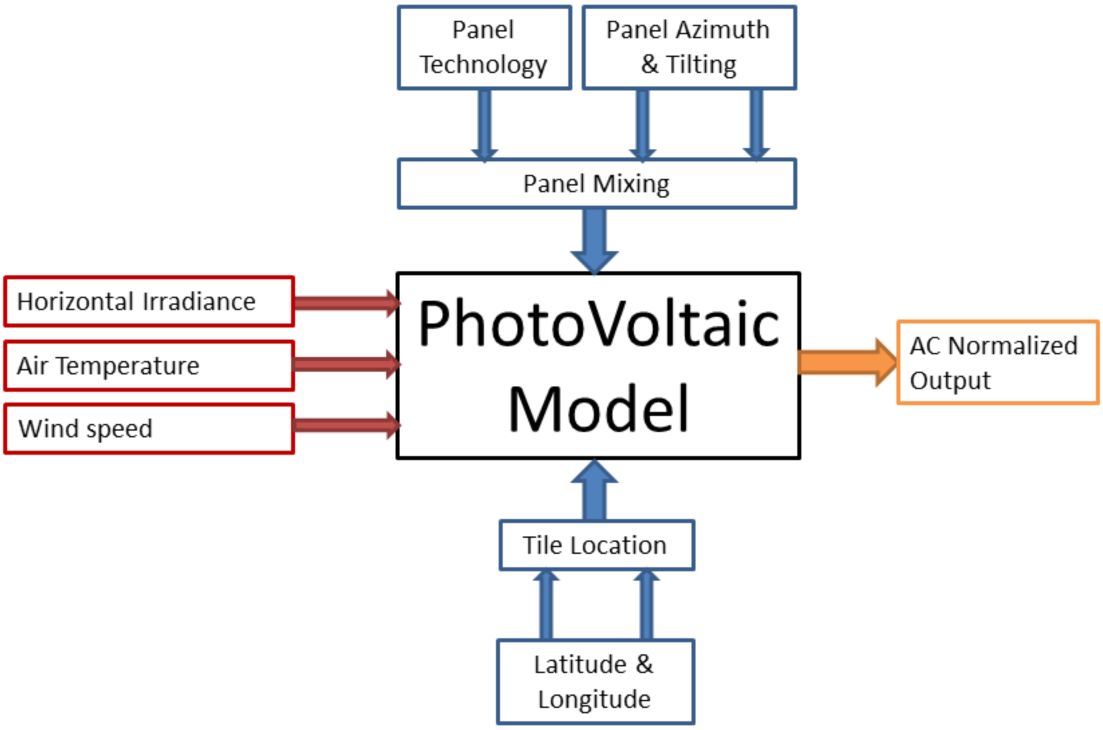

Figure 29: The PV model

The three main inputs can be seen in the left part of the picture and are the horizontal irradiance, the air temperature and the wind speed, given on hourly basis. By the knowledge of the geographic coordinates of each MetCell (called also tile) it is possible to evaluate the movement of the Sun and thus to evaluate the incidence irradiance on the panel. The panels can be installed with different orientations (or azimuth: south, east, west) and different inclination (or tilting: plain, pitched roof, vertical) and for each layout the output is evaluated. The relative distributions between the different compass orientations and tilt angles are given by weighting factors, between 4 representative classes. A reasonable mix of the panel layouts has been chosen and the overall output has been weighted.

Table 7: The 4 classes representing the various orientations and tilting of the PV panels.

Class	Azimuth (-90 East; 0 North; +90 West)	Tilting (0 horizontal; 30 optimal)	Weighting Factor (%)
Horizontal	0	0	30
Optimal – North	0	30	60
Optimal – ENE	-60	30	5
Optimal – WNW	60	30	5

The panel model has been tuned in accordance with the data provided by some manufacturers and considering the experience acquired from the PV installed in the SYSLAB laboratory of the DTU Risø Campus. The DC power produced by the module mainly depends on the incident irradiance and on the temperature, which for instance is function of air temperature, windspeed and irradiance itself. Given that the nominal data are provided for standard meteorological conditions (1000 W/m^2 and 25 °C) for evaluating the reduction from the nominal efficiency, it has been evaluated the dependence of the panel output with different sunlight intensity and the dependence in function of the temperature.

Once the Panel DC output is evaluated it is normalized by considering the nominal power of the module itself and in order to evaluate the AC output, it is necessary to make some assumption on the energy conversion chain, which includes several technical and non-technical losses:

- Panel dirtiness (cannot be neglected especially for polluted area).
- DC cable losses.
- String mismatch (can be significant for big plants).
- Panel shadowing.
- Inverter Efficiency curve (including the insulation transformer, which can be internal or external to the inverter).

Finally, given the mixing of the different panel layouts, the AC normalized output for the MetCell is calculated.

5.3 Simulation Process

The simulation process starts with loading one year of data for all the 10x10 km^2 tiles. After that data series for one year are run through the simulation model for each tile under a node. The nodes are defined by a list of latitude and longitude coordinates of each tile belonging to the specific node. This process is then repeated consecutively for all the nodes.

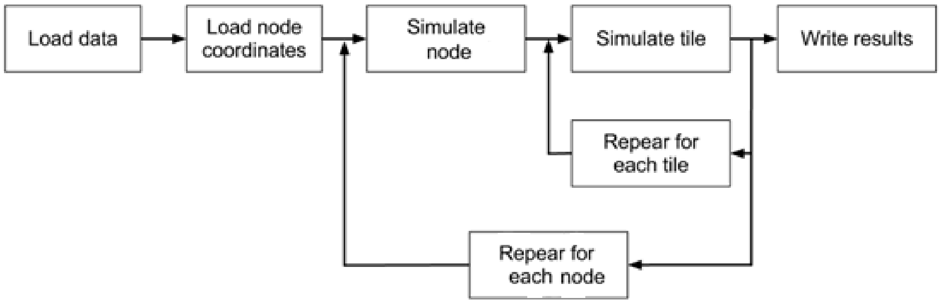

Figure 30. Simulation Process Flow.

5.4 Results

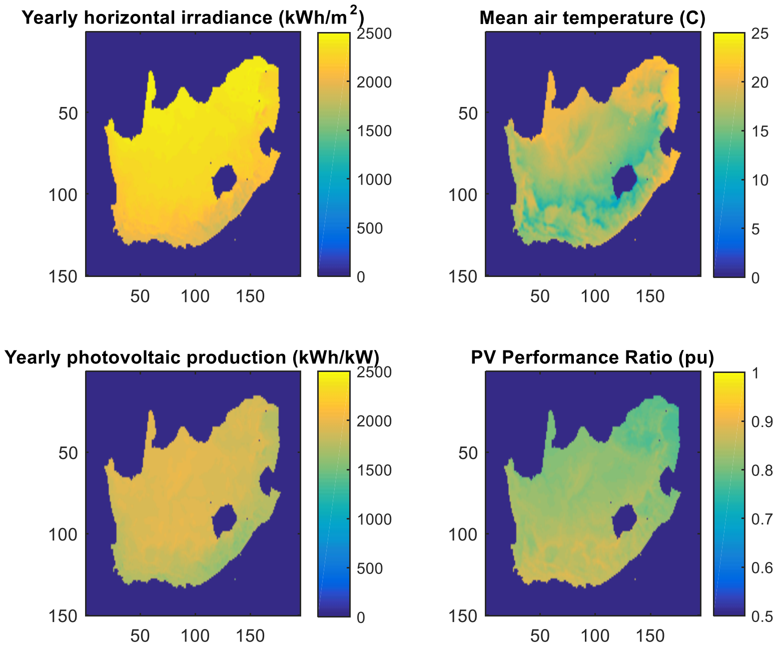

Figure 31. overview results for year 2014. Top left plot: yearly horizontal irradiance (kWh/kW); top right plot: mean air temperature (C); bottom left plot: yearly photovoltaic production (kWh/kw); bottom right plot: PV performance ratio (pu)

Figure 31 reports a snapshot of the results over 2014. The yearly horizontal irradiance is the integral over the year of the hourly irradiance (i.e. cumulated energy received on the ground) and is the main input of the model. The yearly photovoltaic production is the integral over the year of the computed normalized PV production. Values are expressed in kWh per kW nominal power (it is basically the capacity factor).

Two points have to be remembered when it comes to the detailed hourly values:

- Data are in UCT/GMT time, which is 2 hours in advance to South Africa time

- Values (horizontal irradiance and normalized PV production) are cumulated values till the end of the hour. It means that the values shown below in Figure 32, which nominally refers to GMT 5 and GMT 6 am, have to be read as the integral value of irradiance and PV production at the end of each hour (i.e., respectively from 4:01 to 5:00 and from 5:01 to 6:00)

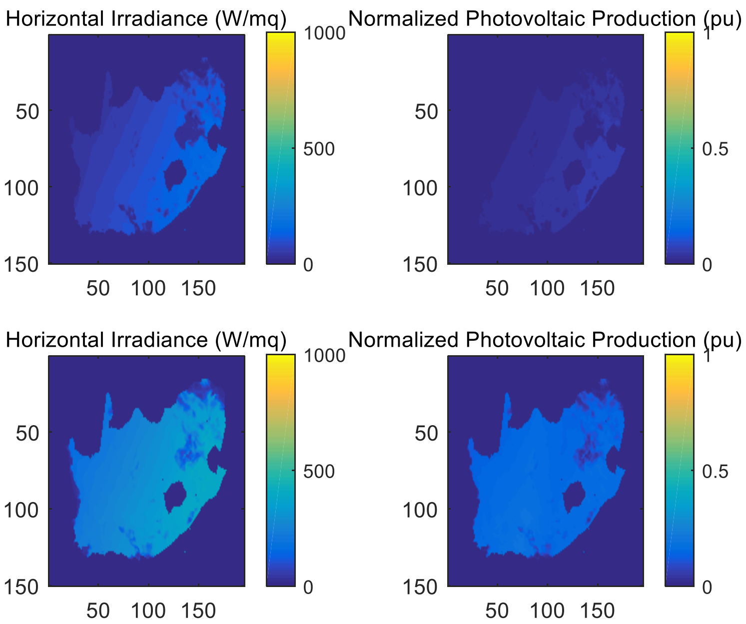

Figure 32. Left plots: horizontal irradiance at 5 and 6 am UCT (cumulated values till the end of the hour). Right plots: normalized PV production at 5 and 6 am UCT (cumulated values till the end of the hour)

The data reported in Figure 32 relates to the 1st of January 2014. In that period of the time, the Sun rises in Durban (east coast) at 5:00 local time (i.e. at 3 am UCT) and rises in Cape town (West coast) at 5:39 local time. It is therefore reasonable to expect very low horizontal solar radiation levels till the 4th value of the time series (i.e. the value that includes results from 3:01 to 4:00 UCT (6:00 local time).

Peak times are reached around noon (10 UCT) as it can be appreciated from Figure 33. The sun sets at 19 local time (i.e. 17 UCT) in Durban, and at 20 in Cape town.

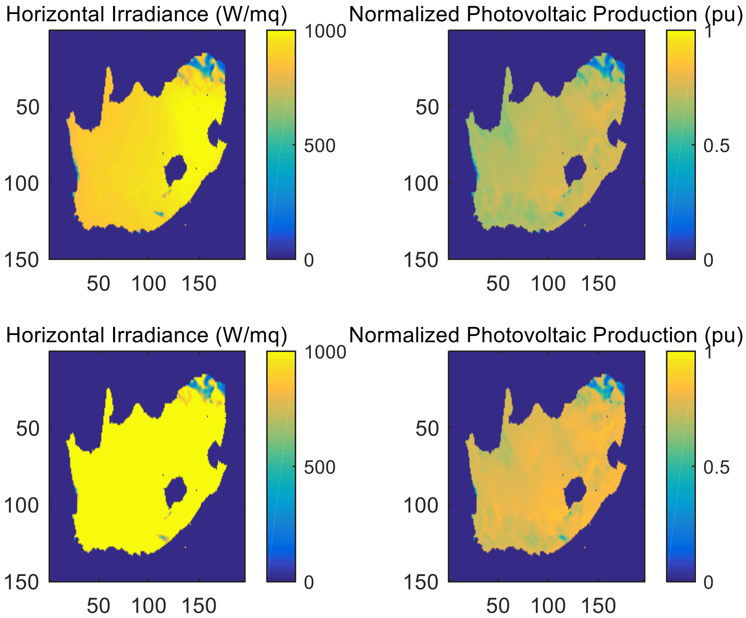

Figure 33. Left plots: horizontal irradiance at 9 and 10 am UCT (cumulated values till the end of the hour). Right plots: normalized PV production at 9 and 10 am UCT (cumulated values till the end of the hour)

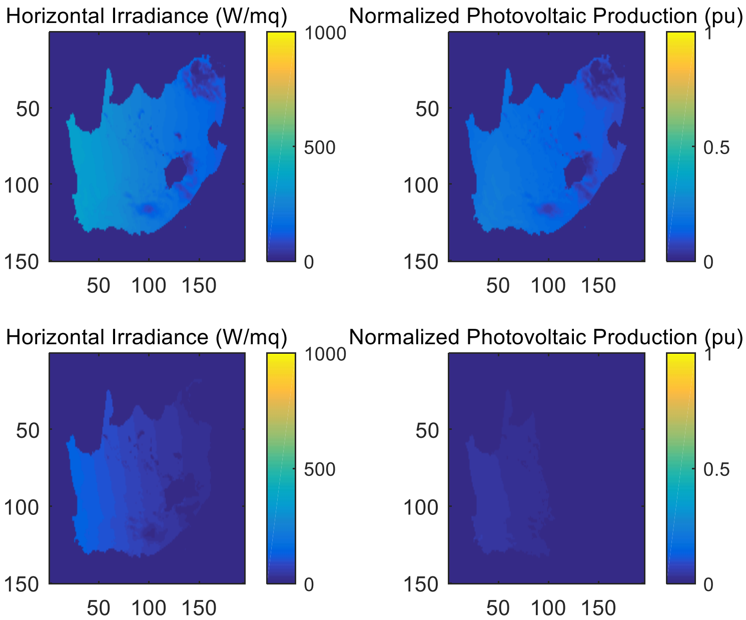

Figure 34. Left plots: horizontal irradiance at 17 and 18 UCT (cumulated values till the end of the hour). Right plots: normalized PV production at 17 and 18 UCT (cumulated values till the end of the hour)

6. Assessment of needs for reserves

6.1 Reserve categories

This section describes how the CorWind time series simulations are used to assess the use of reserves caused by wind power variability and prediction uncertainties. The focus is on the fast (online) reserves, whereas the need for backup capacity is studied in WP3 by project partner Ea Energy Analyses using the stochastic system adequacy tool SISYFOS.

According to the WP1 report [3], The South African Ancillary Services Technical Requirements [29] details the requirements for different reserve categories and specifies five categories of reserves, as follows:

- **Instantaneous reserves** – Used to arrest the frequency at acceptable limits following a contingency.
- **Regulating reserves** – Used for second-by-second balancing of supply and demand, and under AGC control.
- **10-minute reserves** – To balance supply and demand for changes between the Day-ahead market and real-time, such as load forecast errors and unit unreliability.
- **Emergency reserves** – Used when the interconnected power system (IPS) is not in a normal condition, and to return the IPS to a normal condition while slower reserves are being activated.
- **Supplemental reserves** – Used to ensure an acceptable day-ahead risk.

Table 8 shows a summary of requirements to response time (understood as reaction time plus rise time) based on the Ancillary Services Technical Requirements and the ESKOM presentation in the reserves workshop [30].

Table 8: Maximum response (reaction + rise) time and minimum duration of reserve categories

Reserve category	Activation	Max response time	Min duration
Instantaneous	Automatic	10 s	10 min
Regulating	Automatic	10 min	1 h
10 minutes	Manual	10 min	2 h
Emergency	Manual	10 min	2 h
Supplemental	Manual	6 h	2 h

6.2 Activation of reserve categories due to unbalances

Figure 35 illustrates the use of reserve categories in the case of a contingency disturbance. The automatic instantaneous reserves respond very fast to the frequency changes. The automatic regulating reserves also start reacting quite fast to the imbalance and thus reducing the frequency deviation and releasing the instantaneous reserves. Finally, if there are not sufficient automatic reserves available then the operator will manually activate 10 minute reserves to replace the automatic reserves.

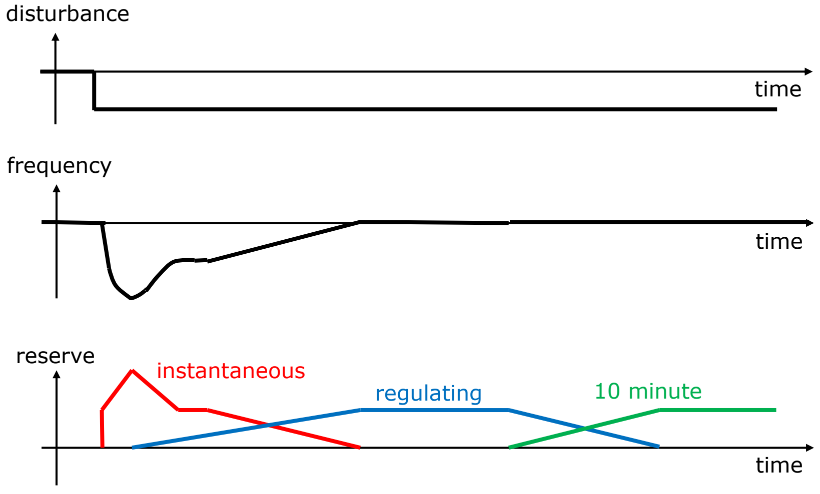

Figure 35.Illustration of use of different reserve categories in the case of a contingency disturbance.

In the case of load or wind power ramping, then the use of reserves is different as illustrated in Figure 36. Initially, the frequency will ramp down much slower because the initial imbalance is quite small. With this small frequency change, the instantaneous reserves will not be activated because the frequency is inside the deadband of the governor. Instead, the regulating reserves will balance the variation with a small time delay. Again, if the imbalance causes the available automatic reserves to be insufficient then the operator will manually activate 10 minute reserves to replace the regulating reserves.

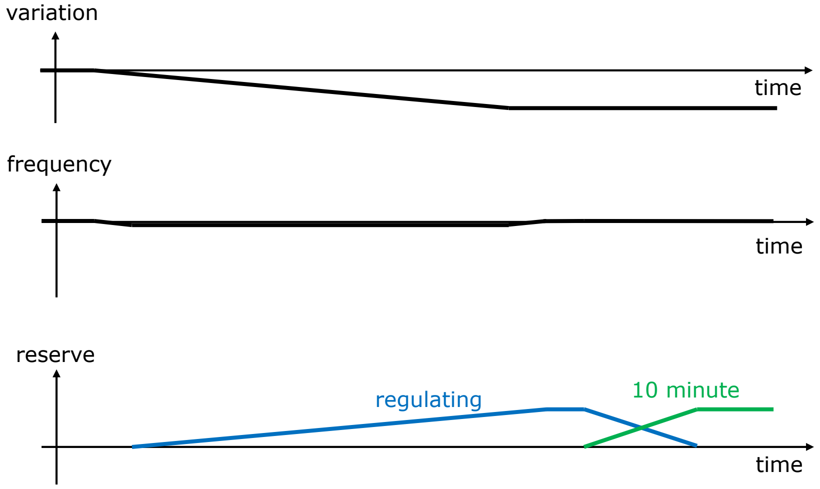

Figure 36.Illustration of use of different reserve categories in the case of a load or wind power ramping.

From these illustrations it is observed that the wind power variability is not affecting the use of instantaneous reserves. Therefore, the impact of wind power variability on instantaneous reserves is disregarded.

6.3 Influence of wind on regulating reserve requirements

According to the Ancillary Services Technical Requirements, regulating reserves should be sufficient to cover the genuine load variations within the hour. In order to quantify the load variations, the ten minute load pickup and load drop off are calculated. In order not to include the steepest deterministic (and therefore predictable) diurnal variations, the approximately 5 % largest load variations are removed and the load variation is determined as the maximum of the remaining approximately 95%.

The present practice is to consider the load equal to the consumption, i.e.

$$P_{\mathrm{load}} = P_{\mathrm{cons}} \tag{6}$$

In order to take the impact of wind and other variable generation into account, the variations of the total (sometimes denoted residual) load should be considered instead of the pure consumption. The total load is defined as

$$P_{total} = P_{cons} - P_{wind} \tag{7}$$

The relation (7) between power also applies to the corresponding ten minute load pickup and load drop off, which is mathematically the same as the ramp rates used to quantify wind power variability in chapter 4. It is now assumed that the 10 minute ramp rates of wind power is uncorrelated with the ten minute load pickup and load drop off. Then the relation between the standard deviations of the ramp rates become

$$\sigma_{total} = \sqrt{{\sigma_{cons}}^2 + {\sigma_{wind}}^2} \tag{8}$$

The present practice and the need for regulating reserves are determined by the load variations, which are regularly analysed and updated by ESKOM. In the present requirements where variable generation is not considered, the (approximately 95%) load variations are varying between 400 MW and 650 MW [29].

If the ramp rate distributions were Gaussian then the relation (8) between standard deviations would apply to any quantiles. For the purpose of the present analysis, this is assumed to be approximately the case for the 95% quantile, i.e.

$$p_{total95} \approx \sqrt{{p_{cons95}}^2 + {p_{wind95}}^2} \tag{9}$$

The 95% quantiles of the 10 minute wind power ramp rates in Figure 23 are given in Table 9 for each scenario case year.

Table 9: 10 min wind power ramp rate 95% quantiles

Case year	2014	2020	2025
95% percentile [p.u.]	-0.062	-0.028	-0.021
95% percentile [MW]	-29	-107	-155

Table 10 shows the impact of wind power on the total need for reserves. First two rows show the latest calculations of the reserves needed to cover the consumption variations from 2015/16 to 2019/20 [29]. The next line is the wind variations for each of the years, interpolating between the absolute value of the wind power quantiles from Table 9 in 2014 and 2020. Next, the total variations are calculated according to according to (9). Finally the increase due to wind is calculated as the difference between the total variations and the consumption variations, both in MW and in % of the original consumption variations. It is seen that the increased need for reserves is less than 10 MW and less than 2% in the entire 5 year period from 2015/16 to 2019/20.

Table 10: Calculation of total need for reserves including wind variations from 2015/16 to 2019/20

Period		2015/16	2016/17	2017/18	2018/19	2019/20
Consumption variations [MW]	Summer	450	450	500	500	550
	Winter	550	550	600	600	650
Wind variations [MW]	-	48	61	74	87	100
Total variations [MW]	Summer	453	454	505	508	559
	Winter	552	553	605	606	658
Increase due to wind [MW]	Summer	3	4	5	8	9
	Winter	2	3	5	6	8
Increase due to wind [%]	Summer	0.7	0.9	1.0	1.6	1.6
	Winter	0.4	0.5	0.8	1.0	1.2

Table 11 show the same calculations for the scenario case years. In order to do this, the consumption variations were extrapolated using the pattern of the regulating reserve requirements in [29]. It is seen that the impact of taking wind power into account is an increase of the requirements to regulating reserves with 2.4% in summer 2025.

Table 11: Calculation of total need for reserves including wind variations in 2014, 2020 and 2025

Period		2014	2020	2025
Consumption variations [MW]	Summer	400	550	700
	Winter	500	650	800
Wind variations [MW]	-	29	106	155
Total variations [MW]	Summer	401	560	717
	Winter	501	659	815
Increase due to wind [MW]	Summer	1	10	17
	Winter	1	9	15
Increase due to wind [%]	Summer	0.3	1.8	2.4
	Winter	0.2	1.4	1.9

The estimated 1.9 % - 2.4 % 2025 increase in Table 11 is significantly less than the 3 % - 7 % increase presented in the Final Workshop [31]. The reason for this difference is that the increase in consumption variations was not included in the workshop presentation which assumed 400 – 650 MW consumption variations.

Since the consumption variations were given with 50MW resolution, it is likely that the above calculated increases due to wind power would not have affected the result with this resolution. On the other hand, it would be good practice to include the impact of wind power variations in future updates of the technical requirements.

6.4 Influence of wind on 10-minute reserve requirements

As it is seen in Figure 36, the 10-minute reserve shall be activated to replace the regulating reserves shortly after they are activated. This brings the system back to a secure normal state with sufficient automatic reserves.

The practice in Denmark is that power is traded day-ahead by the Independent Power Producers (IPPs) on the common Nordic power exchange, Nord Pool. After the day-ahead trade, the balancing responsible IPPs can trade on the Elbas intra-day market. Finally, the Danish TSO Energinet.dk plans the balancing on an hour-ahead basis using the NOIS (Nordic Operation Information System) list, which is a common Nordic regulating power list including bids from Danish, Norwegian, Swedish, and Finnish players.

It is understood that the generation in South Africa is also scheduled day-ahead, which means that the day-ahead forecast error will have to be balanced. Balancing due to contingencies will typically be done intra-day as soon as possible possible using supplemental reserves. However, it should be noticed that early intra-day balancing based on updated wind power forecasts have a risk of being counterproductive if the balancing is done too early. Therefore, hour-ahead balancing is generally recommended for wind power forecast errors, but of course this has to be assessed by the operator in the individual cases.

With the South African reserve categories from clause 6.1, most of the day-ahead wind power forecast errors will therefore be balanced by 10-minute reserves. Table 12 shows the MAE of the day-ahead wind power forecast error which must be balanced.

Table 12: Day-ahead forecast errors (MAE)

Case year	2014	2020	2025
Installed [MW]	460	3800	7400
Day-ahead error [%]	7.5	4.7	4.3
Day-ahead error [MW]	35	179	318

6.5 Use of HA forecasts reducing regulating reserve needs

A forecast system which is able to provide online forecasts to the operator enables the TSO to make an updated power plan, for instance hour-ahead as it is practice in the Danish power system. Using the South African reserve categories, the impact of such an hour-ahead plan will be to reduce the use of the expensive regulating reserves replacing them less costly 10-minute reserves.

The potential for using hour-ahead planning is illustrated in Figure 37 in the case of perfect HA plans. It should be noted that perfect HA plans are of course not realistic, but the example illustrates the idea of replacing the regulating reserves with

The main advantages of replacing regulating reserves with 10-minute reserves are:

- Regulation reserves require investment costs to link the generation plant automatically to the AGC system while 10-minute reserves are called manually.
- Regulation reserves must be reserved before the day-ahead power planning while 10-minute reserves can be called upon when needed.
- Regulation reserves are paid even if they are not activated while 10-minute reserves are only paid when called upon.

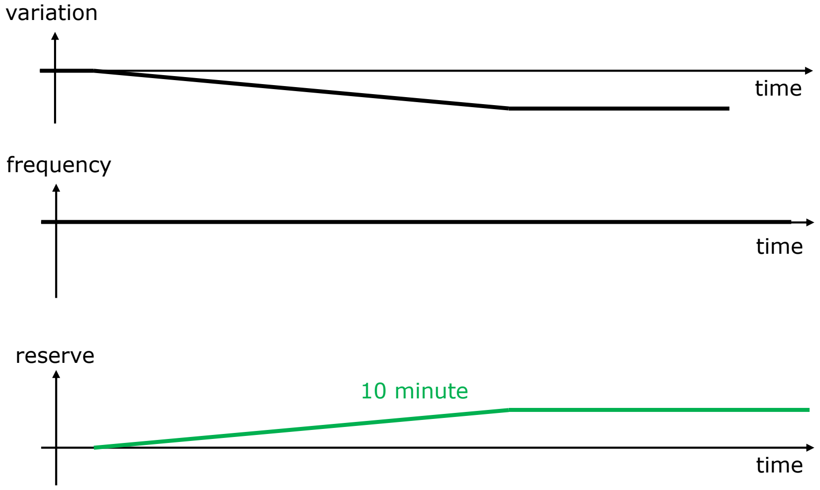

Figure 37.Illustration of use of reserve categories in the case of perfect HA plans.

In reality, a perfect HA plan illustrated in Figure 37 cannot be achieved because of the inevitable HA forecast errors. But the benefit of HA planning is that the imbalance due to forecast errors will be reduced from the DA horizon to the HA horizon. Table 13 quantifies the reduction of the wind power forecast error going from the HA horizon to the DA horizon. It should be noted that the use of HA planning will rely on a good forecast system, not only for wind power but also for consumption, PV generation and other variables in the power system.

Table 13: Mean absolute wind power forecast errors (MAE)

Case year	2014	2020	2025
Installed [MW]	460	3800	7400
Day-ahead error [MW]	35	179	318
Hour-ahead error [MW]	25	118	200
Error reduction [MW]	10	61	118

7. Summary, conclusions and recommendations

7.1 Summary

The main results are:

- The ability of CorWind to simulate wind power time series with realistic variability has been validated by comparison of duration curves for simulated and measured 30 minutes wind power ramp rates of the sum of eight WPPs in South Africa.
- A general wind power curve is estimated based on historical power generation date and WRF weather data.
- CorWind is applied to simulate real and forecasted wind power in 3 simulation cases: the past (2014), planned (2020) and future (2025). For comparison, the time series are normalised with the assumed installed capacities 469 MW in 2014, 3800 MW in 2020 and 7400 MW in 2025.
- High resolution (5 min) real and forecasted wind power time series are aggregated to the system level to study the impact on use of fast reserves.
- Low resolution (1h) wind power time series are aggregated for WP3 to the MTS level
- A PV model is applied to simulate normalised PV power time series with hourly resolution within the borders of South Africa. The PV power time series are provided with 10 km x 10 km resolution in the first place, and subsequently aggregated to MTS level for the WP3 studies.

7.2 Conclusions

The main conclusions of the work are

- The normalized wind power ramp rates of the real wind power is reduced significantly from 2014 to 2020 and further reduced in 2025 because of the spatial smoothening.
- The normalized day-ahead, hour-ahead and online wind power forecast errors are reduced significantly from 2014 to 2020 and further reduced in 2025 because of the spatial smoothening.
- Wind power variability will not impact the use of instantaneous reserves because of the moderate rate of change of wind power combined with the frequency deadband.
- Wind power variability is estimated to increase the use of regulating reserves with max 1.8% in 2020 and max 2.4% in 2025. Those numbers are less than the 50 MW resolution used in the South African technical requirements to ancillary services, but they may still have a minor impact on the future assessments of the need for regulating reserves.
- The use of 10-minute reserves is expected to increase to balance the day-ahead wind (and PV) power forecast errors. The wind power forecast errors have been quantified, but the total need for 10-minute reserves has not been studied in the present work.

7.3 Recommendations

The main recommendations of the work are:

- Include wind and PV in future updates of load variation study determining the need for regulating reserves in the technical requirements to ancillary services.
- Consider HA planning to reduce need for regulating reserves. The cost benefits of HA planning should be assessed taking into account the investment and operation cost of regulating and 10 minute reserves respectively and the possible reduction in forecast errors which are found in the present work.
- HA planning would require to be supplemented with accurate HA forecast system including consumption, wind and solar and adjustment according to online SCADA inputs.

8. References

[1] State of renewable energy in South Africa. Department of Energy, South Africa 2015.

[2] Electricity generated and available for distribution (Preliminary). Statistical release P4141. Statistics South Africa February 2015.

[3] Work package 1 – System reserves in the South African Power System and International Utilities. Part of Strategies about system adequacy and reserve margin with increasing level of variable generation. SANEDI 18 February 2016.

[4] W. Wang, C. Bruyere, M. Duda, J. Dudhia, D. Gill, H-C. Lin, J. Michaelakes, S. Rizvi, and X. Zhang. WRF-ARW Version 3 Modeling System User's Guide. Mesoscale & Microscale Meteorology Division, National Center for Atmospheric Research, Boulder, USA, 2009.

[5] G. L. Mellor and T. Yamada. 1982: Development of a turbulence closure model for geophysical fluid problems, Rev. Geophys. and Space Phys., 20, 851-875.

[6] A.N. Hahmann, D. Rostkier-Edelstein, T. T. Warner, Y. Liu, F. Vandenberg, R. Babarsky, and S. P. Swerdlin, 2010: A reanalysis system for the generation of mesoscale climatographies. J. Appl. Meteor. Climatol., 49, 954-972.

[7] Hahmann A.N., Lennard C., Argent B., Badger J., Vincent C.L., Kelly M.C., Volker P.J.H., Refslund J., 2014b. Mesoscale modeling for the wind atlas for South Africa (WASA) Project. Technical Report, DTU Wind Energy, Roskilde, Denmark

[8] Hahmann, A.N., Vincent, C.L., Peña, A., Lange, J. and Hasager, C.B., 2014a: Wind climate estimation using WRF model output: method and model sensitivities over the sea. International Journal of Climatology, 10.1002/joc.4217.

[9] Dee, D.P. et al., 2011. The ERA-Interim reanalysis: configuration and performance of the data assimilation system. Quart. J. Roy. Meteorol. Soc. 137 (656), 553–597.

[10] R. W. Reynolds, N. A. Rayner, T. M. Smith, D. C. Stokes, and W. Q. Wang. An improved in situ and satellite SST analysis for climate. J. Climate, 2002, 15, 1609–1625

[11] IEC 61400-12-1. Wind turbines – Power performance measurements of electricity producing wind turbines. Ed. 1.0. Geneva 2005-12-16.

[12] B N Aparicio. Aggregated power curve for multiple wind turbines in power system area. Master Thesis. Technical University of Denmark, August 2013.

[13] Project "Software development of CorWind" funded by DTU Wind Energy 2016.

[14] L.J. Fingersh and K.E. Johnson. Baseline Results and Future Plans for the NREL Controls Advanced Research Turbine. 23rd ASME Wind Energy Symposium, Reno, Nevada, January 2004.

[15] P. Nørgaard and H. Holttinen. A multi-turbine power curve approach. Nordic wind power conference, Gothenburg March 2004.

[16] A. Vitina, S. Lüers, A.K. Wallasch, V. Berkhout, A. Duffy, B. Cleary, L. I. Husabø, D. E. Weir, R. Lacal-Arántegui, M. M. Hand, E. Lantz, K. Belyeu, R. Wiser, M. Bolinger, B. Hoen. IEA Wind Task 26: Wind Technology, Cost, and Performance Trends in Denmark, Germany, Ireland, Norway, the European Union, and the United States: 2007–2012. NREL June 2015.

[17] P Sørensen and A Abrahamsen. Wind power. Part of DTU International Energy Report 2015 – Energy systems integration for the transition to non-fossil energy systems. Edited by H H Larsen and L S Petersen. Technical University of Denmark, 2015.

[18] H. Stade, "Spatiotemporal Analysis of Wind Power Forecast Error in Denmark," Master Thesis. Technical University of Denmark, 2014.

[19] N. Cutululis, A. Altiparmakis, M. Litong-Palima, N. Detlefsen and P. Sørensen, " Market and system security impact of the storm demonstration in task-forces TF2. TWENTIES Deliverable D16.6," 2013.

[20] A. Hansen, A. Orths, K. Falk and N. Detlefsen, "Danish Fossil Independent Energy System 2050 - From Strategic Investigations to Intra-Hour Simulation of Balancing Issues," in Wind Integration Workshop, Aarhus, 2011.

[21] M. Marinelli, P. Maule, A. Hahmann, O. Gehrke, P. Nørgård and N. Cutululis, "Wind and Photovoltaic Large-Scale Regional Models for hourly production evaluation," IEEE Transactions on Sustainable Energy, 2014.

[22] G. León, M. Halat, R. Llopis, K. Das, P. Sørensen, R. Moreno, V. Trovato, R. Leelaruji, L. Vanfretti, B. SD, H. DF, J. Turunen and S. Cole, "Improvement of defence plans in European power systems - Proposed harmonization, coordination and inclusion of renewables, distributed resources and PMU information. iTesla Deliverable D6.2 Ed1," 2015.

[23] P. Sørensen, N. Cutululis, A. Vigueras-Rodriguez, L. Jensen, J. Hjerrild, M. Donovan and H. Madsen, "Power Fluctuations from Large Wind Farms," IEEE Trans on Power Systems, 2007.

[24] X. Larsén, S. Ott, J. Badger, A. Hahmann and J. Mann, “Recipes for Correcting the Impact of Effective Mesoscale Resolution on the Estimation of Extreme Winds,” American Meteorology Society, vol. 51, p. 521–533, 2012.

[25] P. Sørensen, A. Hansen and P. Rosas, “Wind models for simulation of power fluctuations from wind farms,” J. Wind Eng. Ind. Aerodyn., vol. 90, pp. 1381-1402, 2002.

[26] L. Söder, “Simulation of wind speed forecast errors for operation planning of multiarea power systems,” in Probabilistic Methods Applied, Ames, 2004.

[27] WRF wind power forecasts for South Africa. http://veaonline.risoe.dk/wasa/

[28] Integrated resource plan for electricity 2010-2030 – Revision 2. Final report March 2011.

[29] Ancillary Services Technical Requirements 2015/16 – 2019/20. Rev. 1 ESKOM 28-10-2014.

[30] Marathon Ntusi. Introduction to Eskom Reserves / Operational Planning. Presented at project Eskom Reserves and System Adequacy Workshop. Johannesburg 2-4 December 2015.

[31] Poul Sørensen, Marisciel Litong-Palima, Andrea Hahmann, Mattia Marinelli. Renewables and need for reserves. Presented at the project Final Workshop Johannesburg 24-25 may 2016.